ChemMedChem

Chemistry Europe
European Chemical Societies Publishing

Accepted Article

Title: Modelling and phenotypic screening of NAP-6 and 10-Cl-BBQ, AhR ligands displaying selective breast cancer cytotoxicity in vitro

Authors: Jennifer R. Baker, Brett L. Pollard, Andrew J. S. Lin, Jayne Gilbert, Stefan Paula, Xiao Zhu, Jennette A. Sakoff, and Adam McCluskey

To be cited as: *ChemMedChem* 10.1002/cmdc.202000721

Link to VoR: https://doi.org/10.1002/cmdc.202000721

WILEY-VCH

WILEY-VCH

FULL PAPER

Modelling and phenotypic screening of NAP-6 and 10-Cl-BBQ, AhR ligands displaying selective breast cancer cytotoxicity *in vitro*

Jennifer R. Baker,[a] Brett L. Pollard,[a] Andrew J. S. Lin,[a] Jayne Gilbert,[b] Stefan Paula,[c] Xiao Zhu,[d] Jennette A. Sakoff *[b] and Adam McCluskey *[a]

[a] Dr JR Baker (0000-0002-9560-301X), Mr BL Pollard (0000-0002-5148-9665), Dr AJS Lin (0000-0001-5558-2261) and Prof A McCluskey (0000-0001-7125-863X)
Chemistry, School of Environmental & Life Sciences
The University of Newcastle
University Drive, Callaghan, NSW 2308, Australia
E-mail: Adam.McCluskey@newcstle.edu.au
[b] Dr J Gilbert (0000-0001-5034-386X) and Dr JA Sakoff (0000-00020-7009-5792)
Experimental Therapeutics Group, Department of Medical Oncology
Calvary Mater Hospital
Edith Street, Waratah NSW 2298, Australia.
[c] Prof S Paula (0000-0003-4100-1467),
Department of Chemistry
Purdue University, 560 Oval Drive, West Lafayette Indiana USA.
[d] Dr. X. Zhu (0000-0003-4946-2081),
Research Computing, Information Technology at Purdue (ITaP),
Purdue University, 155 South Grant Street, West Lafayette, IN (USA)
* Equal author contribution

Supporting information for this article is given via a link at the end of the document.

Abstract: To exploit the interaction of the aryl hydrocarbon receptor (AhR) pathway in developing breast cancer specific cytotoxic compounds, we examined the breast cancer selectivity and the docking pose of the AhR ligands (Z)-2-(2-aminophenyl)-1*H*-benzo[*de*]isoquinoline-1,3(2*H*)-dione (NAP-6; **5**) and 10-chloro-7*H*-benzo[*de*]benzo[4,5]imidazo[2,1-*a*]isoquinolin-7-one (10-Cl-BBQ; **6**). While the breast cancer selectivity of **5** *in vitro* is known, we discuss the SAR around this lead, and show for the first time using phenotypic cell line screening and the MTT assay that **6** also presents with breast cancer selectivity**,** notably in the triple negative (TN) receptor breast cancer cell line MDA-MB-468, the ER+ breast cancer cell lines T47D, ZR-75-1 and the HER2+ breast cancer cell line SKBR3 (GI_{50} values of 0.098, 0.97, 0.13 and 0.21 μM, respectively). Indeed, **6** is 55-fold more potent in MDA-MB-468 cells than the normal MCF10A breast cells (GI_{50} of 0.098 vs 5.4 μM) and more than 130-fold more potent than in cell lines derived from pancreas, brain and prostate (GI_{50} of 0.098 vs 10-13 μM). Molecular docking poses of **5** and **6** together with analogue synthesis and phenotypic screening show the importance of the naphthalene moiety, and an ortho-disposed substituent on the *N*-phenyl moiety for biological activity.

Introduction

Breast cancer is the most commonly diagnosed cancer in women. Early detection is rewarded with good long term survival however, metastatic disease is aggressive and incurable with a 5 year survival of only 25% [4]. Early stage disease is treated with surgery and radiotherapy while aggressive disease is treated with chemotherapy, and hormonal and targeted therapies. Hormone sensitive tumours can be treated with Tamoxifen and anastrozole while Herceptin is used in HER-2 (human epidermal growth factor receptor) positive tumours [1,2]. Failure to respond to treatment is reported in 70% of patients with HER2-positive cancer, and resistance is noted with Tamoxifen and anastrozole [3]. Tumours lacking the estrogen (ER), progesterone (PR), and HER2 receptors, i.e. the triple negative breast cancers (TN), are highly heterogenous and present a significant therapeutic challenge [4,5].

The arylhydrocarbon receptor (AhR) belongs to the basic-helix-loop-helix transcription factor family. The AhR forms a complex with heatshock protein 90, prostaglandin E synthase 3, and a single molecule of the immunophilin-like protein hepatitis B virus X–associated protein 2. Its movement within cells is controlled by binding of the AhR nuclear translocator (ARNT). This binding affords an AhR-ARNT heterodimer complex, culminating in downstream activation of CYP-1A1, -1A2, and -1B1 [6,7]. The CYP1s enact critical metabolic steps for the deactivation and excretion of toxins (and endogenous substrates) [8].

In humans the AhR has a major role in the modulation of the effects of environmental toxins such as benzo[*a*]pyrene (**1**) and 2,3,7,8-tetrachlorodibenzo-*p*-dioxin (**2**) (Figure 1) [6-9]. The AhR also modulates the effects of endogenous ligands, e.g. tryptophan and prostaglandins [10,11]. AhR function is acknowledged as complex and can be activated in both the presence and absence of endogenous and/or exogenous ligands affecting gene transcription [10,12]. The AhR can also induce non transcription factor actions such as Src kinase activation and direct interaction with other receptor signalling pathways [13].

In recent work from our laboratory we have exploited the published link between the AhR pathway and breast cancer initiation and progression in the development of potentially therapeutic small molecules [14-21]. Notable efforts by others have identified aminoflavone (**3**) which progressed to clinical trials [22]. Our efforts have generated the halogenated aryl hydrocarbon (HAH) ANI-7 (**4**) and the polyaryl hydrocarbon (PAH) (*Z*)- 2-(2-aminophenyl)-1*H*-benzo[*de*]isoquinoline-1,3(2*H*)-dione (NAP-6) (**5**) as two small molecules displaying high levels of specificity towards breast cancer cell lines and activation of the AhR pathway (Figure 1).

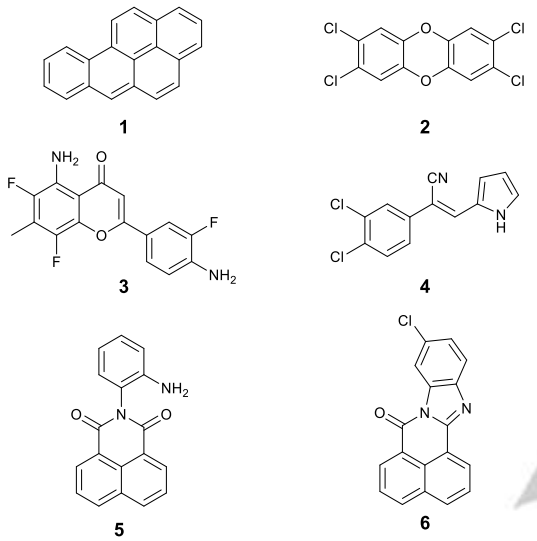

Figure 1. Selected aryl hydrocarbon receptor ligands: benzo[*a*]pyrene (**1**), 2,3,7,8-tetrachlorodibenzo-*p*-dioxin (**2**), aminoflavone (**3**), ANI-7 (**4**), (*Z*)-2-(2-aminophenyl)-1*H*-benzo[*de*]isoquinoline-1,3(2*H*)-dione (NAP-6) (**5**) and 10-chloro-7*H*-benzo[*de*]benzo[4,5]imidazo[2,1-*a*]isoquinolin-7-one (10-Cl-BBQ) (**6**).

Encouraged by our recent discoveries and our application of an in-house AhR homology model in the design of these analogues we turned our attention to 10-Cl-BBQ (**6**) (Figure 1). This compound is a known ligand of AhR [23], and in essence is a hybrid of ANI-7 and NAP-6 with the core scaffold combining the aryl halogen of the acrylonitrile with the polyaromatic rings of the naphthalimide. Our aim was to explore the SAR and breast cancer selectivity of **5** and **6** for the development of breast cancer selective agents [21].

Results and Discussion

In the first instance we compared the cytotoxicity of **4** and **5** with that of **6** in a broad panel of cancer cell lines including HT29 (colon), U87 and SJ-G2 (glioblastoma), MCF-7 (breast), A2780 (ovarian), H460 (lung), A431 (skin), Du145 (prostate), BE2-C (neuroblastoma), MIA-PaCa2 (pancreas) and SMA560 (spontaneous murine astrocytoma) cell lines, and in a select panel of breast cancer cell lines MCF-7, BT474, T47D, ZR-75-1, SKBR3 and MDA-MB-468, BT20 and MDAMB-231 together with the non-cancer breast cell line MCF10A (Table 1). As previously shown for **4** [14] and **5** [21]; **6** presented with significant selectivity towards the growth inhibition of breast cancer cell lines. Indeed, **6** was more potent in the triple negative cell line MDA-MB-468 than **4** or **5,** with a GI_{50} value of 0.098 compared with 0.23 and 0.43 μM, respectively. Notwithstanding this, **6** was also potent in the ER+ breast cancer cell lines T47D, ZR-75-1 and the HER2+ breast cancer cell line SKBR3 (GI_{50} values of 0.97, 0.13 and 0.21 μM, respectively). In fact, **6** was 55-fold more potent in MDA-MB-468 cells than the normal MCF10A breast cells (GI_{50} of 0.098 *vs* 5.4 μM) and more than 130-fold more potent than in cell lines derived from pancreas, brain and prostate (GI_{50} of 0.098 *vs* 10-13 μM). This is the first time that the breast cancer selectivity of **6** has been identified.

The core scaffold of **5** and **6**, with limited synthetic handles to easily introduce a range of substituents, was not readily amenable to rapid focused library development. Thus, we explored the *in silico* docking of **5** and **6** in our AhR homology model to identify more accessible compounds [20] (Figure 2). Inspection of **6** docked within the ligand binding site of the AhR homology model revealed a predominately hydrophobic pocket buried in the interior of the receptor. This is consistent with the nature of the known AhR ligands (Figure 1) [10,22,24]. The binding site is lined by a number of hydrophobic residues including Phe21, Phe27, Leu34, Phe50, Met66, Leu79, Ala93, Ile105 and Val107, creating a non-polar environment capable of generating hydrophobic interactions. Evaluation of docking results conducted with **6** suggested that the compound formed key π-π stacking interactions from one of the naphthalene rings to His63 and His17 within the hydrophobic binding pocket, plus a hydrogen bond between a hydrogen on the aromatic ring and Met66. The hydrogen bond with Met involves an aromatic ring hydrogen atom as the donor and the sulfur atom lone pairs of the methionine side chain as the acceptor. This is not a standard ("canonical") H-bond and is analogous to C-H···O interactions that are sometimes described as "weak" hydrogen bonds. Whereas these bonds tend to be generally weaker than standard hydrogen bonds, their strength increases if polycyclic rings are involved, which is the case here. Moreover, a very tight fit between ligand and receptor was observed, which implies van-der-Waals interactions as an additional contributor to binding.

Table 1. Growth inhibition, GI_{50} values (μM), against a broad panel of cancer cell lines and a focused panel of breast cancer cell lines by 10-Cl BBQ (**6**). Data for ANI-7 (**4**) and NAP-6 (**5**) have been included for comparison. (Lower values indicate higher potency).

	Broad Cancer Cell Line Panel								
	HT29	**U87**	**A2780**	**H460**	**A431**	**Du145**	**BE2-C**	**SJ-G2**	**MIA-PaCa2**
Tissue of origin	colon	brain	ovary	lung	skin	prostate	neural	brain	pancreas
ANI-7 [a] **4**	6.0±0.20	36±3	13±2	3.0±0.4	0.51±0.05	27±1	18±2	13±2	42±3

NAP-6 [b] **5**	5.0±0.55	>50	21±4	15±7.5	0.25±0.12	>50	>50	>50	>50
10-Cl-BBQ **6**	4.0±0.72	7.6±2.0	4.1±0.5	10±2.0	0.82±0.20	13±0.58	5.8±0.78	13±1.5	10±0.7

	Breast Cancer Cell Line Panel								
	MCF-7	**BT474**	**T47D**	**ZR-75-1**	**SKBR3**	**MDA-MB468**	**BT20**	**MDA-MB-231**	**MCF10A**
Classification	ER+ [c]	ER+	ER+	ER+	HER2 [d]	TN [e]	TN	TN	normal [f]
ANI-7 [a] **4**	0.38±0.03	1.0±0.3	0.16±0.02	0.18±0.02	0.21±0.03	0.23±0.01	1.0±0.4	17±4	26±3
NAP-6 [b] **5**	0.70±0.12	0.43±0.07	0.18±0.02	0.12±0.03	0.22±0.02	0.43±0.07	14±1.5	35±3	31±1.5
10-Cl-BBQ **6**	5.8±1.1	>10	0.97±0.3	0.13±0.04	0.21±0.06	0.098±0.04	>10	>10	5.4±1.2

[a] Gilbert et al 2018; [b] Gilbert et al 2020; [c] estrogen receptor (ER) positive; [d] human epidermal growth factor positive (HER2); [e] triple negative for ER, progesterone (PR) and HER2 receptors; [f] normal breast cell line.

As our, and Punj's prior reports have clearly identified ANI-7, NAP-6 and 10-Cl-BBQ all elicit their breast cancer specificity through the AhR [15, 21, 25], we sought to examine these compounds and the analogues produced herein in our previously reported AhR homology model. Analysis of the docking of **6** suggested that the benzimidazole moiety afforded no meaningful interactions within the AhR binding site, with the possible exception of attractive van-der-Waals interactions. Additionally, no substantive interaction with the carbonyl moiety was evident. Combined, these data suggested that significant scaffold simplification with retention of activity may be feasible. Our scaffold simplification approach suggested three key components that in principle could give rise to Libraries A, B and C which could be rapidly investigated (Figure 3).

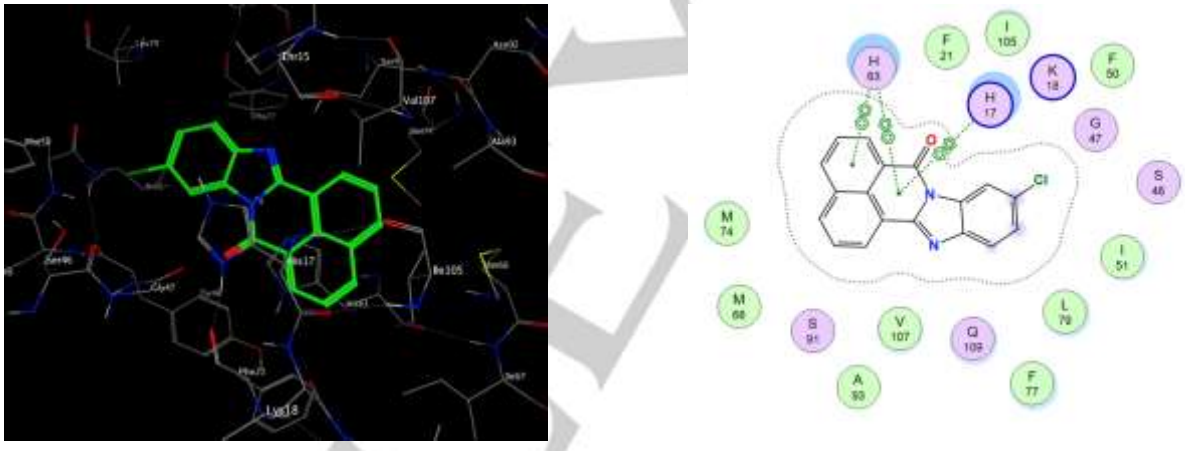

A **B**

Figure 2. **A**) Docked pose of 10-Cl-BBQ (**6**) bound in the AhR PAS-B domain homology model, illustrating the central and buried nature of the ligand binding site. Residues are shown as wire frame and coloured by atom type. **B**) A 2D generated ligand interaction diagram of the AhR PAS-B domain, shown with 10-Cl-BBQ (**6**) docked. Hydrophobic residues are shown in green; hydrophilic residues are shown in purple; the green dashed line depicts π-π and H-bond interactions.

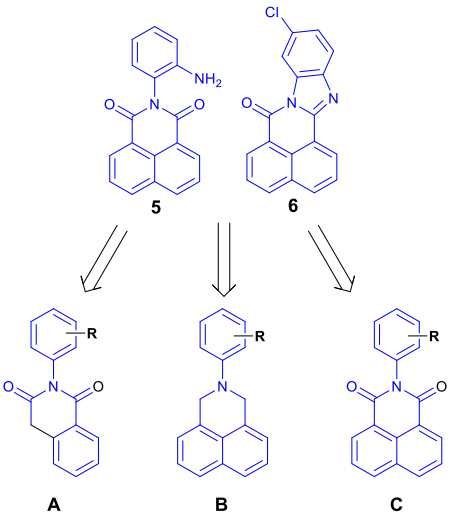

Figure 3. Potential focused Libraries A, B and C arising from the simplification of the core structure of NAP-6 (**5**) and 10-Cl-BBQ (**6**) The structures in blue are those that are shared with the parent structures.

We have previously reported the synthesis of a wide variety of anhydride modified analogues as clathrin, dynamin and protein phosphatase inhibitors [26-29], the chemistry of which permitted rapid access to focused libraries that would enable SAR acquisition. Of the three analogue types identified, Library A addresses the importance of the second naphthyl aromatic moiety; Library B the importance of the *N*-imide substituent, in engaging with the AhR binding pocket; and Library C the nature of the *N*-imide carbonyl interactions. Commencing with Library A, a 3-membered focused library retaining the chlorophenyl moiety of **6** was synthesised on treatment of homophthalic anhydride (**7**) with 2-, 3-, and 4-chloroaniline (**8**-**10**) to afford the corresponding imides **11**-**13** in good yields (see Experimental). These analogues were screened in a broad cancer screening panel comprising HT29 (colon), U87 and SJ-G2 (glioblastoma), MCF-7 (breast), A2780 (ovarian), H460 (lung), A431 (skin), Du145 (prostate), BE2-C (neuroblastoma), MIA-PaCa2 (pancreas) and SMA560 (spontaneous murine astrocytoma) cell lines, as well as the normal breast cell line MCF10A. Initial screening was conducted at 25 μM and these data are presented in Table 2.

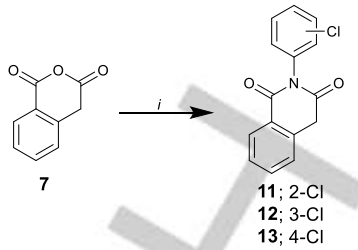

Scheme 1. Reagents and conditions: i) 2-, 3-, 4- chloroaniline (**8**-**10**), AcOH, 24h, Δ.

From analysis of the data presented in Table 2, the scaffold simplification (removal of one of the naphthyl phenyl rings) of **6** afforded no analogue with notable cytotoxicity against any of the cancer cell lines evaluated. As a result we next turned our attention to the synthesis of Library B analogues, which most closely resemble leads **5** and **6**. In this series, as with the Library A analogues, the chlorophenyl moiety was retained. Compound access was afforded by either an ethanol reflux with catalytic trimethylamine, or heating in the room temperature ionic liquid [BMIM][Br], from 1,8-naphthalic anhydride (**14**) and chloroanilines (**8**-**10**) (Scheme 2) [27]. The 2-chloro moiety was synthetically inaccessible presumably due to a combination of electronic effects and steric clashes with the naphthalic anhydride functionality; the more planar structure of the naphthalimide backbone (for **15**), compared to the more flexible homophthalic moiety (for **11**), resulted in steric hindrance that significantly affected the reaction rate; however, the 3- and 4-chloro derivatives were successfully afforded. The initial Library B analogues comprised naphthalic *N*-imides (**16**-**17**), with the screening data presented in Table 3.

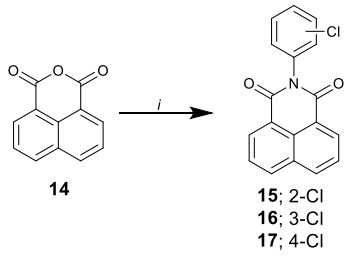

Scheme 2. Reagents and conditions: i) 2-, 3-, 4- chloroaniline (**8**-**10**), Et_3N, EtOH, 18 h, Δ; or 2-, 3-, 4- chloroaniline (**8**-**10**), [BMIM][Br], 1 h, Δ.

Table 2. Percent cell growth inhibition in response to 25 μM of drug, against a panel of cancer cell lines by homophthalic imides **11**-**13**. (Higher values indicate higher potency).

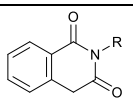

R	HT29	U87	MCF-7	A2780	H460	A431	Du145	BE2-C	SJ-G2	MIA-PaCa2	SMA560	MCF10A
 **11**	*10±2*	*<10*	*20±12*	*17±6*	*10±2*	*14±1*	*<10*	*<10*	*16±3*	*<10*	*nd*	*<10*
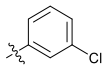 **12**	*21±2*	*<10*	*38±1*	*21±6*	*15±3*	*<10*	*<10*	*23±2*	*17±7*	*14±3*	*nd*	*12±6*

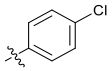 **13**	*15±6*	*<10*	*14±6*	*27±8*	*<10*	*<10*	*<10*	*10±3*	*13±1*	*11±4*	*nd*	*<10*

nd = not determined

Table 3. Growth inhibition, GI_{50} values (μM), against a panel of cancer cell lines by naphthalene imides **16**-**30**. Low values indicate higher potency. Data in italics is percentage growth inhibition at a fixed 25 μM compound concentration (higher values indicate higher potency).

R	HT29	U87	MCF-7	A2780	H460	A431	Du145	BE2-C	SJ-G2	MIA-PaCa2	SMA560	MCF10A
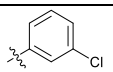 **16**	4.5±0.10	19±4.2	3.3±0.71	7.5±0.60	15±1.8	5.4±0.61	15±2.3	7.8±1.4	9.2±0.67	6.9±0.18	nd	6.4±0.59
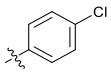 **17**	27±7.4	30±2.0	21±9.5	23±7.4	32±0.0	29±1.0	37±4.5	24±0.0	30±0.5	31±1.0	nd	21±5.8
 **18**	*<10*	*<10*	*<10*	*13±1*	*<10*	*10±1*	*<10*	*<10*	*<10*	*<10*	*nd*	*<10*
 **19**	*<10*	*nd*	*24±5*	*<10*	*10±4*	*<10*	*<10*	*<10*	*14±1*	*<10*	*<10*	*nd*
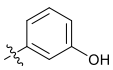 **20**	*16±7*	*nd*	*49±10*	*11±3*	*34±7*	*15±3*	*<10*	*18±5*	*12±3*	*10±3*	*<10*	*nd*
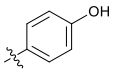 **21**	*36±3*	*nd*	*71±6*	*38±4*	*42±3*	*23±4*	*51±3*	*63±4*	*39±3*	*55±0*	*20±2*	*nd*
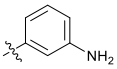 **22**	*<10*	*nd*	*21±3*	*<10*	*14±4*	*<10*	*<10*	*21±6*	*11±3*	*12±4*	*10±3*	*nd*
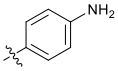 **23**	-[b]	-	-	-	-	-	-	-	-	-	-	-
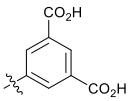 **24**	*16±7*	*nd*	*16±4*	*<10*	*11±3*	*<10*	*<10*	*<10*	*<10*	*<10*	*<10*	*nd*
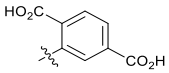 **25**	*13±5*	*nd*	*21±3*	*<10*	*10±2*	*<10*	*12±6*	*<10*	*<10*	*<10*	*<10*	*nd*
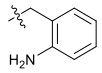 **26**	11±2.3	8.8±4.1	5.0±0.17	8.5±2.8	5.8±0.33	3.3±0.32	3.6±0.70	5.4±1.1	5.8±0.17	6.2±0.67	nd	4.9±0.50
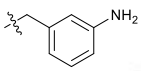 **27**	11±2.4	26±2.8	6.1±2.2	5.3±1.3	11±2.6	4.3±0.96	21±8.0	4.4±1.0	12±6.8	4.9±1.8	nd	4.8±0.30
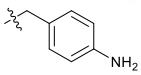 **28**	*43±3*	*nd*	*70±3*	*36±5*	*59±2*	*38±1*	*50±5*	*64±4*	*63±1*	*38±1*	*88±4*	*nd*
 **29**	*<10*	*nd*	*<10*	*<10*	*14±5*	*<10*	*<10*	*<10*	*<10*	*<10*	*<10*	*nd*
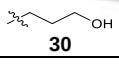 **30**	*14±7*	*nd*	*12±2*	*<10*	*25±4*	*<10*	*<10*	*11±8*	*19±3*	*<10*	*<10*	*nd*

[a] from Gilbert et al, 2020 [b] insoluble in the testing media, nd = not determined.

As with the homophthalic analogues **11**-**13**, the chlorophenyl **16**-**17** displayed only low levels of cytotoxicity at the initial 25 μM compound concentration examined (Table 3). In comparison to **6**, modelling analysis, after docking in our in-house AhR homology model [19], revealed that these compounds only interacted with His63 and Met66 and failed to engage with His17 (Supplementary Information, Figure S1), which could explain their lower activities.

Chlorine moiety removal gave **18** which showed very low levels of cytotoxicity (Table 3), however these data and the insights gained on analysis of the docked poses of **15**-**18** suggested that the introduction of H-bonding moieties capable of interaction with Gln109, Thr15 and Gly47 may increase AhR binding site affinity, and based on our hypothesis, activity against the breast cancer cell line MCF-7 (Figure 2 and Figure 4). Accordingly we synthesised, as described in Scheme 2, three series of analogues with -OH (**19**-**21**), -NH_2 (**22**-**23**) and -CO_2H (**24** and **25**) substituents on the *N*-imide phenyl moiety. Of these eight analogues, 4-NH_2 **23** was insoluble in the assay medium. Of the remaining seven analogues, breast cancer selectivity in MCF-7 cells was observed. Indeed, 2-OH **19**, 3-OH **20** and 4-OH **21** showed the greatest potency in MCF-7 cells with a percentage cell death level of 24%, 49% and 71%, respectively. Interestingly, the amino analogue 3-NH_2 **22** showed none of the potency or selectivity of the parental 2-NH_2 **5**. This is consistent with the predicted AhR mediated cytotoxicity against breast cancer. We do note, however, the inherent risk in drawing hard and fast SAR conclusions from analysis of single datapoint, with these data only circumstantially support our modelling hypothesis. We do note that with the active analogues their cancer cell line response phenocopies that observed with ANI-7, NAP-6 and 10-Cl-BBQ. Their mode of action is thus consistent with activation of the AhR pathway.

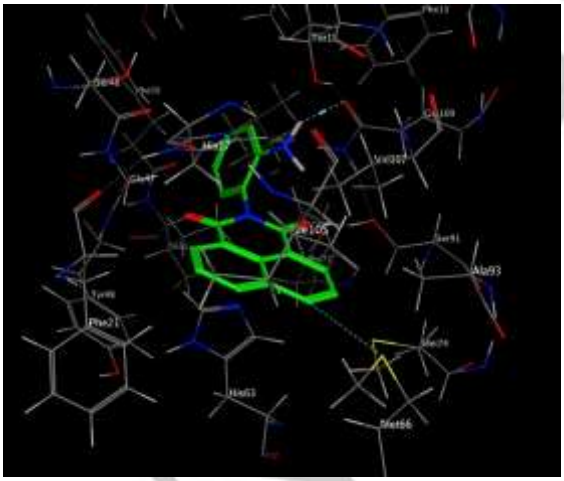

A

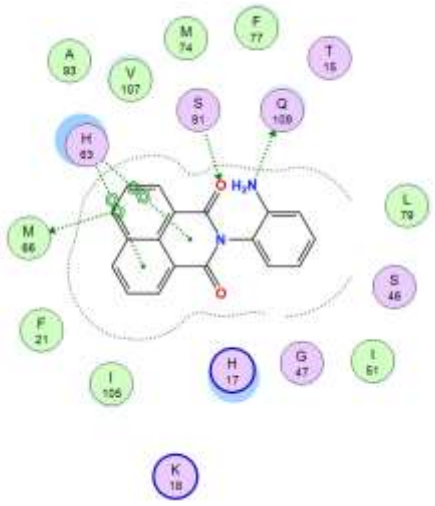

B

Figure 4. A) Docked pose of **5** in the AhR binding pocket with three types of favourable binding interactions evident: π-π interactions between the two rings of the aromatic system of the ligand and His63, a H-bond between a hydrogen atom attached to the aromatic system and Met66, and another H-bond between the 2-NH_2 moiety and Gln109. Residues are shown as wire frame and coloured by atom type. **B**) A 2D generated ligand interaction diagram of the generated AhR PAS-B domain, shown with **5** docked. Hydrophobic residues are shown in green; hydrophilic residues are shown in purple; the green dashed line depicts π-π interactions.

Docking revealed that the compounds adopted a very similar overall ("consensus") orientation (Supporting Information, Figure S2). Subtle differences in a compound's position determined whether certain interactions were present or not. With **5**, the 2-NH_2 moiety results in the *N*-phenyl ring twisting from planarity and this allows access to a strong H-bond with Gln109; this coupled with π–π interactions with the two naphthalene rings to His63 and a H-bond from the aromatic-H to Met66 affords a strong binding site interaction, evidenced by the increased MCF-7 cytotoxicity and the lack of effect with the 3-NH_2 moiety. Due to the symmetry of the molecule, we occasionally observed the H-bond with Gln109 to be substituted by one with Gly47, with all the other interactions remaining the same. The cytotoxicity data obtained with the carboxylate substituted **24** and **25**, is consistent with their AhR binding poses with the carboxylate moiety failing to engage with Gln109 (Supporting Information). From these data, it appears critical that the *N*-phenyl moiety adopts a skewed conformation to allow access to Gln109, and as such the corresponding aminobenzyl amines (**26**-**28**) would be expected to result in a decrease in MCF-7 cytotoxicity, although the increased flexibility imparted by the methylene spacer may off-set this somewhat permitting the aminophenyl moiety to rotate and potentially interact with Gln109. As shown from the cytotoxicity data, the aminobenzyl analogues (**26**-**27**) displayed increased potency with no breast cancer selectivity, while **28** displayed reduced potency but maintained some breast selectivity, possibly due to its ability to interact with Gly47, which is consistent with the above modelling hypothesis.

In a similar manner removal of the phenyl ring and introduction of ethanol (**29**) and propanol (**30**) moieties also resulted in a loss of activity (Table 3). This strongly supports this class of compounds favouring the retention of the naphthalene moiety, and an ortho-disposed substituent on the *N*-phenyl moiety. Further substantiation of the critical nature of the 2-NH_2 moiety was evident on examination of the corresponding 2-CH_3 **31**, with the *in silico* analysis showing the loss of the Gln109 H-bond, and a corresponding loss in cytotoxicity activity. In a similar vein, a 2-pyridyl **32** supports the 2-NH_2 moiety participating in H-bond donation. Pyridyl **32** was inactive in our cancer screening panel. The exception to these observations was with the 2-hydroxy analogue **19**.

According to our docking results, **5** and **19** exhibited the same binding pose and engaged the AhR with the same set of interactions. However, **5** showed good potencies against the cells lines tested whereas **19** was mostly inactive. This was contrary to our docking model predictions. In our previous reports with the phenylacrylonitrile class of compounds with copious data in IC_{50} format (not a mix of IC_{50} and %-inhibition) we noted excellent model to activity correlations [20]. To account for this apparent discrepancy, we subjected the docked poses of both compounds to 100 ns of molecular dynamics (MD) simulations with the introduction of explicit water molecules. Despite being much more demanding on computational resources, MD – unlike docking – does not suffer from limitations due to the neglect of solvent molecules or rigidity of the receptor and can therefore provide a more detailed and realistic picture of the events taking place in the binding site.

Interestingly, the final orientations (average of the last 20 ns of simulation) of both compounds deviated from their docking-predicted poses (Figure 5A and B). The deviation was much larger for **19** than for **5** and could be described as a rotation by approximately 90° around an axis perpendicular to the plane of the central ring of the molecule. A comparison of snapshots from the final stages of the MD simulations that included the roles assumed by water molecules in the binding pocket revealed two distinct patterns (Figure 5C and D). 2-Amino **5** preserved the H-bond to Gln109 and maintained close contacts with Met66 as well as co-planarity with the imidazole ring of His63 while also permitting the presence of two water molecules in the binding site. 2-Hydroxy **19**, on the other hand, was surrounded by three water molecules, one of which formed a bridged H-bond between the hydroxyl group of **19** and Thr15 and His17. This prevents **19** from making a critical H-bond to Gln109. Moreover, the π-π interactions with His63 were absent because of a significant reorientation of the ligand which eliminated the co-planarity of the two entities. This latter perturbation is a direct consequence of the additional water molecule present in the AhR binding pocket with **19**. Presumably, the somewhat smaller size of the hydroxyl group compared to that of the amino group along with slight differences in H-bonding capabilities of these two functional groups allowed **19** to adopt a pose significantly different from that of **5**. This finding was not possible without examination of the molecular dynamics and inclusion of water molecules within this system.

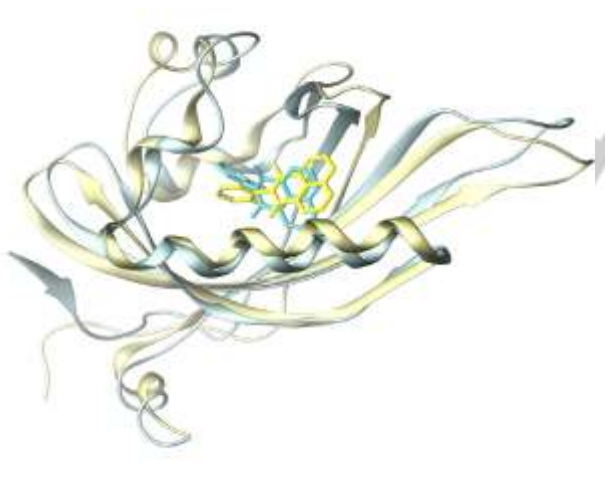

A

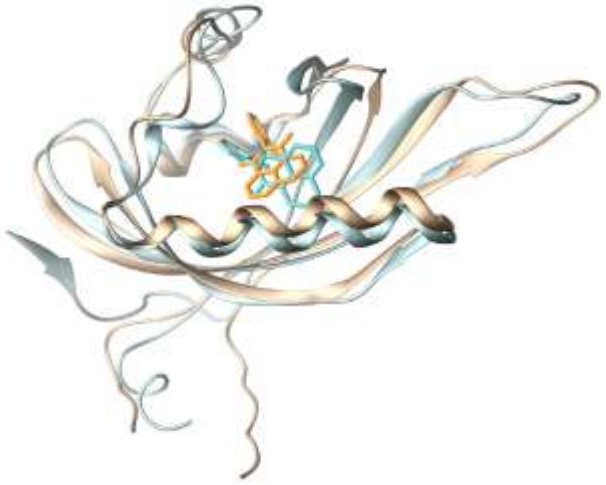

B

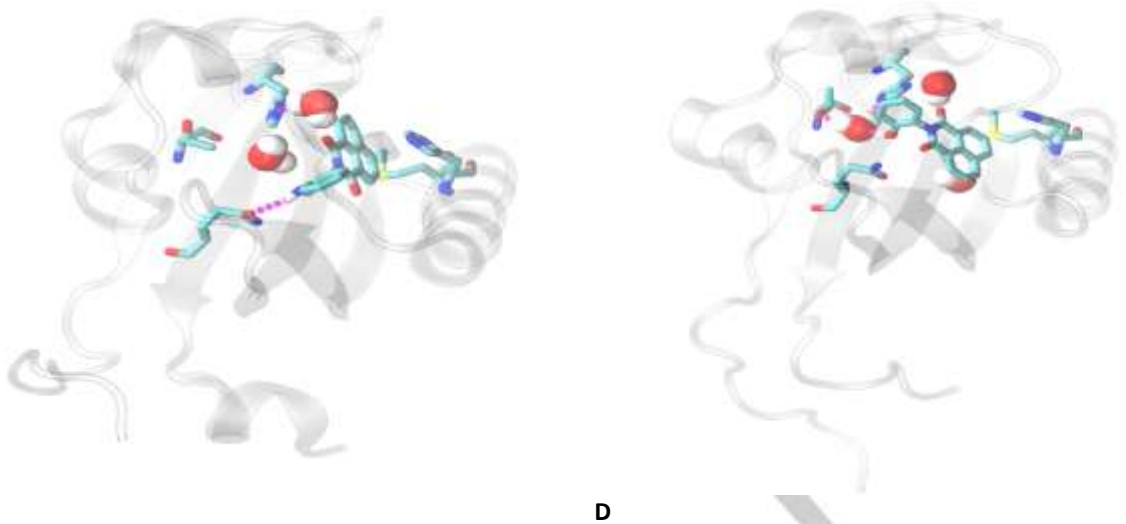

C D

Figure 5. A) Final pose of **5** (yellow, last 20 ns of a 100 ns simulation), **B**) **19** (orange) compared to docking predicted pose (cyan); **C**) Binding pose of **5**; and **D**) **19** with H-bonds and explicit solvent molecules.

As ligand binding is usually accompanied by conformational changes of the receptor, the different binding pose observed for **19** most likely resulted in a different overall conformation of the AhR. This in turn could have had an effect on the interactions between the AhR its protein binding partners and thereby affect the AhR signaling pathway. This assumption was supported by a comparison of RMSD values of the protein backbone, which showed noticeable differences between the two ligand/receptor complexes throughout the duration of the simulations (Supporting Information, Figure S3). Such a scenario would be compatible with only **5** activating the pathway and **19** being unable to do so, despite its ability to bind.

Given our findings with **5**, we revisited our initial homophthalic imide Type A analogues, attempting the synthesis of the equivalent 2-, 3- and 4- amino **34**-**35**, as outlined in Scheme 1. The 3- and 4-amino analogues were unable to be synthesised, with the ring-opened derivative afforded in each instance. The 2-amino analogue (**34**; Supporting Information, Figure S4) was found to be inactive in our cancer screening panel (Supporting Information, Table S1), and on examination of the binding poses, while 2-amino **34** showed a similar twisting of the *N*-phenyl moiety and participation in a H-bond with Gln109, the loss of the aromatic-H H-bond with Met66 and only one π–π interaction with His63 appears to have rendered these analogues poor binders in the AhR binding domain.

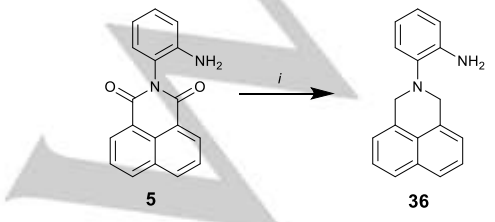

Scheme 3. Reagents and Conditions: i) I_2, $NaBH_4$, THF, 25-60 ºC, 24 h.

Our final synthetic modification accessed a single Type C analogue based on 2-amino **5**. Treatment of **5** with I_2 and $NaBH_4$ afforded the carbonyl free **36** (Scheme 3). This analogue was inactive, supporting an important role for the imide carbonyls in engaging, directly or indirectly, with the AhR binding site.

Examination of the AhR docking poses of **32**, **33** and **36** reveals that with each analogue, key binding interactions are lacking within the AhR binding site (Supporting Information, Figure S4). With 2-pyridyl **32** the predicted binding pose results in loss of part of the π–π interactions with H63 and of H-bond with Gln109; **33** sees the loss of part of the π–π interactions and the H-bonds with Met66 and Gln109; and **36**, the loss of H-bonds with Met66 and Gln109. In each instance, the loss of the aforementioned binding interactions reduces the observed cytotoxicity (Table 2 and Supporting Information, Table S1).

Having defined the SAR for molecule **5**, we now show using inverted light microscopy the significant differential effect of **5** on the induction of cell death in MDA-MB-468 breast cancer cells compared with normal breast cells within 16h of continuous exposure (Figure 6).

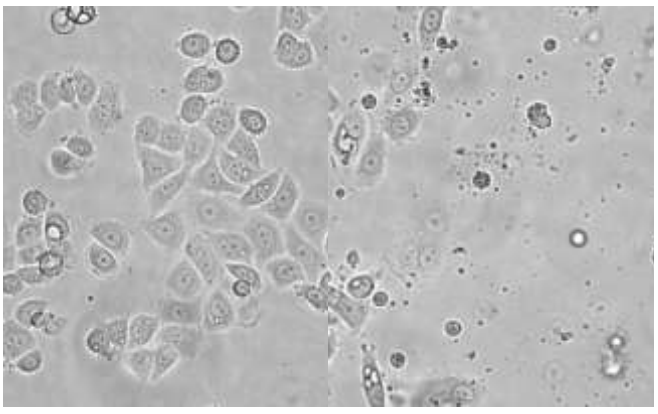

A B

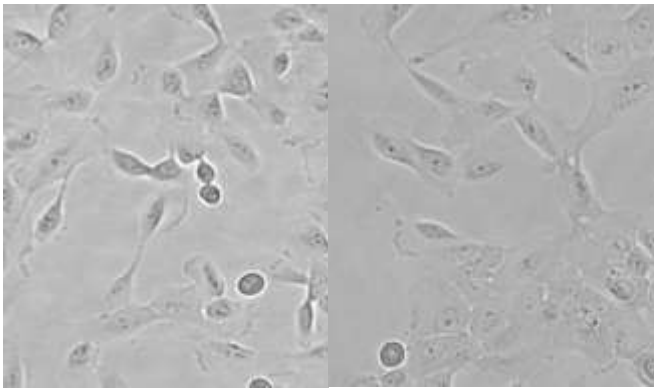

C D

Figure 6. Light microscopy images of MDA-MB-468 (**A,B**) and MCF10A (**C,D**) cells treated with (**B,D**) or without (**A,C**) **5** (50 μM) for 16 h.

Conclusions

Both compounds **5** and **6** have previously been identified as AhR ligands [21, 23], and **5** as a breast cancer selective molecule. Examination of **6** in a broad panel of cancer cell lines and in an expanded panel of breast cancer cell lines revealed, for the first time, comparable breast cancer selectivity to that of **5**. Relative to the broad panel of cancer cell lines, **6** was up to 130-fold more potent in breast cancer cells, and up to 55-fold more potent in breast cancer cells compared with normal breast cells. The greatest potency was 100nM in MDA-MB-468 breast cancer cells. In the drug resistant BT20 and MDA-MB-231 cell lines, the observed activity was more modest at >10 μM. Scaffold simplification approaches with **5** and **6** identified Type A, B and C analogues as potential scaffolds for interaction with the AhR binding site. Subsequent synthesis and screening against a cancer cell line panel revealed that Type A analogues were, to all intentions, devoid of noteworthy cytotoxicity. Examination of Type B analogues revealed potential interactions within the AhR binding site through π-π interactions with His63, and aromatic hydrogen bond with Met66 and a H-bond from the -NH_2 moiety of **5** to Gln109. Removal of one of these interactions was detrimental to activity with the synthesis of homophthalic anhydride derived **33**, 2-pyridyl **32** and the carbonyl free **36** lacking one or more of these binding site interactions effected a loss of cytotoxicity. In each instance the loss of activity was consistent with a subtle change in binding site pose of the respective analogues. Further analysis of 2-hydroxy **19** via molecular dynamic simulations demonstrated that whilst the same interactions were observed with the receptor as with **5**, after 100 ns of solvent-mediated MD, the pose of **19** deviated significantly from the docking-predicted pose, resulting in the loss of the critical interactions previously observed. This effect was only observable via MD simulations with our docking efforts failing to provide an explanation for the observed activity discrepancy.

Collectively these data support the further development of **5** and **6** as potential breast cancer specific agents targeting the AhR pathway.

Experimental Section

Biology

Cell culture and stock solutions

Stock solutions were prepared as follows and stored at -20 °C: drugs were stored as 40 mM solutions in DMSO. All cell lines were cultured in a humidified atmosphere 5% CO_2 at 37 ºC. The cancer cell lines were maintained in Dulbecco's modified Eagle's medium (DMEM) (Trace Biosciences, Australia) supplemented with 10% foetal bovine serum, 10 mM sodium bicarbonate, penicillin (100 IU/mL), streptomycin (100 μg/mL), and glutamine (4 mM). The non-cancer MCF10A cell line was cultured in DMEM:F12 (1:1) cell culture media, 5% heat inactivated horse serum, supplemented with penicillin (50 IU/mL), streptomycin (50 μg/mL), 20 mM Hepes, L-glutamine (2 mM), epidermal growth factor (20 ng/mL), hydrocortisone (500 ng/mL), cholera toxin (100 ng/mL), and insulin (10 μg/mL).

In vitro growth inhibition assay

Cells in logarithmic growth were transferred to 96-well plates. Cytotoxicity was determined by plating cells in duplicate in 100 μL medium at a density of 2500-4000 cells/well in 96 well plates. On day 0, (24 h after plating) when the cells were in logarithmic growth 100 μL medium with or without the test agent was added to each well. After 72 h drug exposure growth inhibitory effects were evaluated using the MTT (3-[4,5-dimethylthiazol-2-yl]-2,5-diphenyltetrazolium bromide) assay with absorbances read at 540 nm. Percentage growth inhibition was determined at a fixed drug concentration of 25 μM. A value of 100% is indicative of complete cell growth inhibition. Those analogues showing appreciable percentage growth inhibition underwent further dose response analysis allowing for the calculation of a GI_{50} value. An eight-point dose response curve was produced, using MS Excel software. Each data point is the mean ±S.E.M. calculated from four to five replicates, which were performed on separate occasions and separate cell line passages. From these dose-response curves, the GI_{50} value was calculated, representing the drug concentration at which cell growth is 50% inhibited based on the difference between the optical density values on day 0 and those at the end of drug exposure [31, 32].

Morphological Assessment: Live cells were examined for morphological alterations after 16 h exposure with and without 50μM **5** using phase contrast microscopy (Olympus CKX41 inverted microscope 100x magnification).

Docking of compounds into the homology model of the AhR PAS-B domain

Development of a homology model for the AhR PAS-B domain

Homology modelling was performed with the suite MOE (Molecular Open Environment, Chemical Computing Group, Montreal, Canada) as described previously. Briefly, the sequence of the human AhR was obtained from the NCBI website (https://www.ncbi.nlm.nih.gov/, accession code NP_001612.1) and only the part corresponding to the PAS-B domain was considered. A homology search with MOE identified the crystal structure 4F3L (a transcriptional activator complex with a basic helix-loop-helix PAS-domain) as the most suitable template (24.8% identity and 48.8% similarity) [33]. Model generation was executed at default settings with the Amber force field. Subsequent analysis of the model's geometry revealed no steric clashes or outliers in backbone bond lengths as well as bond, dihedral, and rotamer angles.

Docking of compounds into the homology model

The structures of all ligands to be docked were constructed in MOE and their conformations energy-minimized using Molecular Mechanics in conjunction with the MMFF94x force field. The binding site for docking

was defined by the position of co-crystallized ligands in related proteins with PAS-B domains, such as 3F1O [34], 3H7W [35], and 3H82 [36], after being superimposed onto the homology model.

Docking was performed using MOE's default settings, using the triangle matcher method in combination with the London dG scoring function for the initial placement of the ligand, followed by a refinement of the 30 top poses with rigid receptor setting and the GBVI/WSA scoring function. Analysis and visualization of the docking output, such as identification of hydrogen bonds, steric clashes, hydrophobic interactions, or π-π interactions were performed in MOE.

Molecular dynamics simulations

The stability of docking-predicted ligand poses was evaluated in molecular dynamics (MD) simulations using the program NAMD (version 2.10) [37]. The simulations were conducted using periodic boundary conditions in all directions. The cut off distance for both Coulombic and van der Waals (vdW) interactions was set at 12 Å, and the force-based switching function was used for the vdW interactions with a switching range of 10–12 Å. Long-range Coulombic interactions were evaluated by the Particle Mesh Ewald method [38]. The temperature was maintained at 303.15 K, controlled by Langevin dynamics, while the pressure was maintained at 1 atm using the Nosé–Hoover Langevin piston method [39]. The bonds with hydrogen atoms were constrained to their equilibrium lengths using the RATTLE algorithm [40]. Simulations were performed with an energy minimization of 10000 steps, six equilibrium stages, totalling 0.75 ns, followed by a production phase of 100 ns with a time step of 2 fs. During the equilibration, all heavy atoms of the protein–ligand complex were harmonically restrained to their initial positions, with an initial force constant of 25 $kcalmol^{-1}$ $Å^{-2}$ that was gradually decreased at each stage. Simulations were visualized with the program VMD [41].

Starting from a docked ligand–receptor pose, the system was solvated, and potassium and chloride ions were added at 150 mM to mimic physiological conditions while preserving charge neutrality. The system was then solvated in a cubic box of water. The dimensions of the box were chosen such that the minimum distance between any atom of the solute and the box walls was 12 Å. All simulations used the CHARMM36 force field for the protein [42] and the ions, and the CHARMM-modified TIP3P model for water molecules [43–47].

The ligand parameters were generated from the CHARMM general force field.

Chemistry

General Methods

All reactions were performed using standard laboratory equipment and glassware. Solvents and reagents were purchased from Sigma Aldrich, Alfa Aesar or AK Scientific and used as received. Organic solvents were of bulk quality, and were distilled from glass prior to use. Organic solvent extracts were dried with magnesium sulfate ($MgSO_4$), and removed under reduced pressure with either Büchi or Heidolph rotary evaporators. Melting points were recorded in open capillaries on a Büchi 565 Melting Point Apparatus. Where available, literature values are provided and appropriately referenced. Electrospray mass spectra were recorded using HPLC-grade 10% acetonitrile/H_2O (with 0.1% formic acid) as carrier solvents on an Agilent Technologies 1260 Infinity UPLC system with a 6120 Quadrupole LC/MS in electrospray ionization (ESI) positive and negative modes. TLC was performed on Merck silica gel 60 F254 pre-coated aluminium plates with a thickness of 0.2 mm. Column chromatography was performed under 'flash' conditions on Merck silica gel 60 (230-400 mesh).

Nuclear magnetic resonance (NMR) spectroscopy was performed on a Bruker Avance III 400 MHz spectrometer, where proton NMR (^{1}H NMR) spectra and carbon NMR (^{13}C NMR) spectra were acquired at 400 and 100 MHz respectively. All spectra were recorded in deuterated dimethyl sulfoxide (DMSO-d_6) or deuterated chloroform ($CDCl_3$) obtained from Cambridge Isotope Laboratories Inc. Chemical shifts (δ) were measured in parts per million (ppm) and referenced against the internal reference peaks. Coupling constants (J) were measured in Hertz (Hz). Multiplicities are denoted as singlet (s), broad singlet (bs), doublet (d), doublet of doublets (dd), triplet (t), quartet (q), triplet of doublets (td), doublet of triplets (dt) and multiplet (m). Peaks are listed in decreasing chemical shift in the following format: chemical shift (integration (1H), multiplicity (1H), coupling constant (1H).

The Biotage® initiator$^+$ was used to perform microwave reactions.

*2-(2-Chlorophenyl)isoquinoline-1,3(2*H*,4*H*)-dione (**11**)*

To a mixture of homophthalic anhydride (**7**) (1.0 mmol, 0.162 g) and 2-chloroaniline (1.5 mmol, 0.191 mL) was added acetic acid (10 mL). This solution was then heated, with magnetic stirring, to 125 ºC for 24 h. The ensuing mixture was cooled to room temperature, then treated with water (30 mL). The resultant precipitate was collected by filtration then dried *in vacuo* to afford the title compound as an off-white solid (0.031 g, 11%), m.p.: 120-122 ºC [47].

^{1}H NMR (400 MHz, $CDCl_3$) δ 8.26 (dd, *J* = 7.9, 1.0 Hz, 1H), 7.66 (td, *J* = 7.6, 1.4 Hz, 1H), 7.59 – 7.55 (m, 1H), 7.51 – 7.48 (m, 1H), 7.44 – 7.39 (m, 2H), 7.37 (d, *J* = 7.7 Hz, 1H), 7.30 – 7.26 (m, 1H), 4.25 (ABq, $\Delta\nu_{AB}$ = 32 Hz, J_{AB} = 22.4 Hz, 2H); ^{13}C NMR (101 MHz, $CDCl_3$) δ 169.3, 164.4, 134.4, 134.3, 133.3, 132.8, 130.6, 130.42, 130.39, 129.7, 128.1, 127.9, 127.6, 125.3, 37.0; IR (cm^{-1}) 1674 (C=O), 743 (C-Cl); LCMS (ESI$^+$) m/z: 272 [M+H]$^+$ (100%), 274 [M+H]$^+$ (35%).

*2-(3-Chlorophenyl)isoquinoline-1,3(2*H*,4*H*)-dione (**12**)*

To a mixture of homophthalic anhydride (**7**) (1.0 mmol, 0.162 g) and 3-chloroaniline (1.5 mmol, 0.191 mL) was added acetic acid (10 mL). This solution was then heated, with magnetic stirring, to 125 ºC for 24 h. The ensuing mixture was cooled to room temperature, then treated with water (30 mL). The resultant precipitate was collected by filtration then dried *in vacuo* to afford the title compound as an off-white solid (0.107 g, 39%), m.p.: 150-153 ºC [47].

^{1}H NMR (400 MHz, $CDCl_3$) δ 8.24 (d, *J* = 7.8 Hz, 1H), 7.66 (t, *J* = 7.8 Hz, 1H), 7.49 (t, *J* = 7.8 Hz, 1H), 7.45 – 7.43 (m, 2H), 7.36 (d, *J* = 7.6 Hz, 1H), 7.24 (s, 1H), 7.12 – 7.11 (m, 1H), 4.23 (s, 2H); ^{13}C NMR (101 MHz, $CDCl_3$) δ 169.8, 164.9, 136.2, 135.0, 134.4, 134.2, 130.4, 129.7, 129.23, 129.22, 128.2, 127.5, 127.1, 125.3, 37.1; IR (cm^{-1}) 1677 (C=O), 742 (C-Cl); LCMS (ESI$^+$) m/z: 272 [M+H]$^+$ (100%), 274 [M+H]$^+$ (35%).

*2-(4-Chlorophenyl)isoquinoline-1,3(2*H*,4*H*)-dione (**13**)*

To a mixture of homophthalic anhydride (**7**) (1.0 mmol, 0.162 g) and 4-chloroaniline (1.5 mmol, 0.191 mL) was added acetic acid (10 mL). This solution was then heated, with magnetic stirring, to 125 ºC for 24 h. The ensuing mixture was cooled to room temperature, then treated with water (30 mL). The resultant precipitate was collected by filtration then dried *in vacuo* to afford the desired compound as an off-white solid (0.123 g, 45%), m.p.: 158-160 ºC [48].

^{1}H NMR (400 MHz, $CDCl_3$) δ 8.24 (d, *J* = 7.8 Hz, 1H), 7.66 (td, *J* = 7.8, 1.3 Hz, 1H), 7.49 (2 overlapping doublets, d, *J* = 8.8 Hz, 2H; other doublet *J* not determined, 1H), 7.35 (d, *J* = 7.8 Hz, 1H), 7.15 (d, *J* = 8.8 Hz, 2H), 4.23 (s, 2H); ^{13}C NMR (101 MHz, $CDCl_3$) δ 169.9, 165.0, 134.9, 134.3, 134.2, 133.6, 130.1 (2C), 129.8 (2C), 129.7, 128.2, 127.5, 125.4, 37.1; IR (cm^{-1}) 1666 (C=O), 743 (C-Cl); LCMS (ESI$^+$) m/z: 272 [M+H]$^+$ (100%), 274 [M+H]$^+$ (35%).

*2-(3-Chlorophenyl)-1*H*-benzo[*de*]isoquinoline-1,3(2*H*)-dione (**16**)*

A solution of 1,8-naphthalic anhydride (**14**) (1.0 mmol, 0.198 g), 3-chloroaniline (3.0 mmol, 0.315 mL) and triethylamine (10 drops) in 15 mL absolute ethanol was heated to reflux for 44 h, with magnetic stirring, then allowed to cool to room temperature. The mixture was filtered *in vacuo*, the yellow precipitate washed with cold ethanol (15 mL) and cold diethyl ether (15 mL), and dried *in vacuo* to afford the desired compound as an off-white solid (0.132 g, 43%), m.p.: 232-234 ºC.

^{1}H NMR (400 MHz, $CDCl_3$) δ 8.65 (d, *J* = 7.0 Hz, 2H), 8.29 (d, *J* = 8.1 Hz, 2H), 7.81 (t, *J* = 7.6 Hz, 2H), 7.48 (m, 7.49 – 7.48, 2H), 7.35 (s, 1H), 7.24 (m, 7.24 – 7.23, 1H); ^{13}C NMR (101 MHz, $CDCl_3$) δ 164.3 (2C), 136.6, 135.1, 134.7 (2C), 131.9 (2C), 130.4, 129.4, 129.2, 128.7, 127.26, 127.25 (2C), 122.7 (3C); IR (cm^{-1}) 1667 (C=O), 774 (C-Cl); LCMS (ESI^+) m/z: 308 $[M+H]^+$ (100%), 310 $[M+H]^+$ (35%); HRMS (ESI^+) m/z calculated for $C_{18}H_{11}ClNO_2$ $(M+H)^+$ 308.0473; compound did not ionise.

*2-(4-Chlorophenyl)-1*H*-benzo[*de*]isoquinoline-1,3(2*H*)-dione (**17**)*

A solution of 1,8-naphthalic anhydride (**14**) (1.0 mmol, 0.198 g), 4-chloroaniline (3.0 mmol, 0.315 mL) and triethylamine (10 drops) in 15 mL absolute ethanol was heated to reflux for 44 h, with magnetic stirring, then allowed to cool to room temperature. The mixture was filtered *in vacuo*, the yellow precipitate washed with cold ethanol (15 mL) and cold diethyl ether (15 mL), and dried *in vacuo* to afford the desired compound as an off-white solid (0.139 g, 45%), m.p.: 282-284 ºC [49].

^{1}H NMR (400 MHz, $CDCl_3$) δ 8.64 (d, *J* = 7.7 Hz, 2H), 8.28 (d, *J* = 7.7 Hz, 2H), 7.80 (t, *J* = 7.7 Hz, 2H), 7.52 (d, *J* = 8.0 Hz, 2H), 7.27 (d, *J* = 8.0 Hz, 2H); ^{13}C NMR (101 MHz, $CDCl_3$) δ 164.4 (2C), 134.8, 134.6, 134.0, 131.90 (2C), 131.87 (2C), 130.2 (2C), 129.8 (2C), 128.7, 127.2 (2C), 122.8 (2C); IR (cm^{-1}) 1701 (C=O), 776 (C-Cl); LCMS (ESI^+) m/z: 308 $[M+H]^+$ (100%), 310 $[M+H]^+$ (35%).

*2-Phenyl-1*H*-benzo[*de*]isoquinoline-1,3(2*H*)-dione (**18**)*

To a mixture of 1,8-naphthalic anhydride (**14**) (0.56 mmol, 0.111 g) and aniline (0.61 mmol, 0.057 g) was added 1-butyl-3-methylimidazolium bromide (0.8 mL). This solution was then heated, with magnetic stirring, to 140 ºC for 18 h. The ensuing mixture was cooled to room temperature, then treated with absolute ethanol (3 mL) before chilling to 0 ºC. The resultant precipitate was collected by filtration *in vacuo*, washed with cold ethanol (4 × 7.5 mL) and cold diethyl ether (3 × 7.5 mL), then dried *in vacuo* to afford the desired compound as a tan crystalline solid (0.153 g, 44%), m.p.: 179 ºC [50].

^{1}H NMR (400 MHz, DMSO-d_6) δ 8.53 (d, *J* = 3.6 Hz, 2H), 8.51 (d, *J* = 2.6 Hz, 2H), 7.91 (t, *J* = 7.8 Hz, 2H), 7.53 (t, *J* = 7.3 Hz, 2H), 7.46 (t, *J* = 7.3 Hz, 1H), 7.40 (t, *J* = 4.2 Hz, 2H); ^{13}C NMR (101 MHz, DMSO-d_6) δ 163.7 (2C), 136.1 (2C), 134.4 (2C), 131.5, 130.7, 129.1, 128.9, 128.2 (2C), 127.9 (3C), 127.3 (2C), 122.6; IR (cm^{-1}) 3050 (Ar-H), 1660 (C=O), 700 (Ar-H); LCMS (ESI^+) m/z: 274 $[M+H]^+$ (100%).

*2-(2-Hydroxyphenyl)-1*H*-benzo[*de*]isoquinoline-1,3(2*H*)-dione (**19**)*

A solution of 1,8-naphthalic anhydride (**14**) (1.0 mmol, 0.198 g), 2-aminophenol (3.0 mmol, 0.327 g) and triethylamine (8 drops) in 15 mL absolute ethanol was heated to reflux for 18 h, with magnetic stirring, then allowed to cool to 0°C. The mixture was filtered *in vacuo*, the pale brown solid washed with cold ethanol (3 mL) and cold diethyl ether (3 mL), and dried *in vacuo* to afford the desired compound as a creamy-coloured solid (0.167 g, 58%), m.p.: 310-312 ºC [51].

^{1}H NMR (400 MHz, DMSO-d_6) δ 9.64 (s, OH), 8.51 (d, *J* = 1.8 Hz, 2H), 8.49 (s, 2H), 7.90 (t, *J* = 7.8 Hz, 2H), 7.30 (t, *J* = 8.1 Hz, 1H), 6.87 – 6.84 (m, 1H), 6.79 - 6.78 (m, 2H); ^{13}C NMR (101 MHz, DMSO-d_6) δ 163.6 (2C), 157.8, 137.0, 134.4 (2C), 131.4, 130.7 (2C), 129.4, 127.8, 127.2 (2C), 122.7 (2C), 119.6, 116.2, 115.2; IR (cm^{-1}) 3243 (O-H), 1645 (C=O), 777 (Ar-H); LRMS (ESI^+) *m/z*: 290 $[M+H]^+$, (100%); (ESI^-) *m/z*: 288 $[M-H]^-$ (100%).

*2-(3-Hydroxyphenyl)-1*H*-benzo[*de*]isoquinoline-1,3(2*H*)-dione (**20**)*

A solution of 1,8-naphthalic anhydride (**14**) (1.0 mmol, 0.198 g), 3-aminophenol (3.0 mmol, 0.327 g) and triethylamine (8 drops) in 15 mL absolute ethanol was heated to reflux for 18 h, with magnetic stirring, then allowed to cool to 0 ºC. The mixture was filtered *in vacuo*, the pale brown precipitate washed with cold ethanol (3 mL) and cold diethyl ether (3 mL), then dried *in vacuo* to afford the desired compound as a creamy-coloured solid (0.166 g, 57%), m.p.: 296-298 ºC.

^{1}H NMR (400 MHz, DMSO-d_6) δ 9.64 (s, OH), 8.51 (d, *J* = 1.8 Hz, 2H), 8.49 (s, 2H), 7.90 (t, *J* = 7.8 Hz, 2H), 7.30 (t, *J* = 8.1 Hz, 1H), 6.87 – 6.84 (m, 1H), 6.79 - 6.78 (m, 2H); ^{13}C NMR (101 MHz, DMSO-d_6) δ 163.3 (2C), 153.4, 134.4 (2C), 131.5, 130.6 (2C), 130.3, 129.6, 127.9, 127.2 (2C), 122.9, 122.7 (2C), 119.1, 116.4; IR (cm^{-1}) 3290 (O-H), 1650 (C=O), 760 (Ar-H); LRMS (ESI^+) *m/z*: 290 $[M+H]^+$, (100%); (ESI^-) *m/z*: 288 $[M-H]^-$ (100%); HRMS (ESI^-) m/z calculated for $C_{18}H_{10}NO_3$ $(M-H)^-$ 288.0666; found: 287.9986.

*2-(4-Hydroxyphenyl)-1*H*-benzo[*de*]isoquinoline-1,3(2*H*)-dione (**21**)*

A solution of 1,8-naphthalic anhydride (**14**) (1.0 mmol, 0.198 g), 4-aminophenol (3.0 mmol, 0.327 g) and triethylamine (8 drops) in 15 mL absolute ethanol was heated to reflux for 18 h, with magnetic stirring, then allowed to cool to 0 ºC. The mixture was filtered *in vacuo*, the dark purple precipitate washed with cold ethanol (3 mL) and cold diethyl ether (3 mL), and dried *in vacuo* to afford the desired compound as a purple-grey solid (0.231 g, 80%), m.p.: 291-293 ºC [52].

^{1}H NMR (400 MHz, DMSO-d_6) δ 9.64 (s, 1H, OH), 8.49 (s, 2H), 8.48 (s, 2H), 7.89 (t, *J* = 7.8 Hz, 2H), 7.14 (dt, *J* = 8.8, 2.8 Hz, 2H), 6.87 (dt, *J* = 8.8, 2.8 Hz, 2H); ^{13}C NMR (101 MHz, DMSO-d_6) δ 163.9 (2C), 157.1, 134.3 (2C), 131.4, 130.7 (2C), 129.1 (2C), 127.8, 127.2 (2C), 126.9, 122.7 (2C), 115.4 (2C); IR (cm^{-1}) 3280 (O-H), 1648 (C=O), 781 (Ar-H); LRMS (ESI^+) *m/z*: 290 $[M+H]^+$, (100%); (ESI^-) *m/z*: 288 $[M-H]^-$ (100%).

*2-(3-Aminophenyl)-1*H*-benzo[*de*]isoquinoline-1,3(2*H*)-dione (**22**)*

A solution of 1,8-naphthalic anhydride (**14**) (1.34 mmol, 0.266 g), *m*-phenylenediamine (4.38 mmol, 0.474 g) and triethylamine (10 drops) in absolute ethanol (20 mL) was heated to reflux, with magnetic stirring, for 36 h. Upon cooling to room temperature, the mixture was filtered *in vacuo*, and the resultant yellow precipitate was washed with ethanol (2 × 15 mL) cold diethyl ether (2 × 15 mL), and dried *in vacuo* to afford the desired compound as a yellow solid (0.308 g, 80%), m.p.: >250 ºC (decomp.).

^{1}H NMR (400 MHz, DMSO-d_6) δ 8.50 (s, 2H), 8.48 (s, 2H), 7.89 (t, *J* = 8.0 Hz, 2H), 7.13 (t, *J* = 8.0 Hz, 1H), 6.65 (d, *J* = 8.0 Hz, 1H), 6.51 (s, 1H), 6.48 (d, *J* = 12.0 Hz, 1H), 5.23 (bs, NH_2); ^{13}C NMR (101 MHz, DMSO-d_6) δ 163.5 (2C), 149.4, 136.6, 134.3 (2C), 131.4, 130.7 (2C), 129.1 (2C), 127.8, 127.2 (2C), 122.6, 116.0, 114.3, 113.6; IR (cm^{-1}) 3411 (NH_2), 3348 (NH_2), 2971 (Ar-H), 1658 (C=O), 776 (Ar-H); LCMS (ESI^+) m/z: 289 $[M+H]^+$ (100%); HRMS (ESI^+) m/z calculated for $C_{18}H_{13}N_2O_2$ $(M+H)^+$ 289.0972; found: 289.0973.

*2-(4-Aminophenyl)-1*H*-benzo[*de*]isoquinoline-1,3(2*H*)-dione (**23**)*

A solution of 1,8-naphthalic anhydride (**14**) (0.99 mmol, 0.198 g), *p*-phenylenediamine (3.13 mmol, 0.339 g) and triethylamine (10 drops) in ethanol (15 mL) was heated to reflux, with magnetic stirring, for 20 h. After cooling to room temperature, the mixture was filtered *in vacuo*, and the reddish-brown precipitate was washed with ethanol (20 mL) and cold diethyl ether (20 mL), and dried *in vacuo* to afford the desired

compound as a mustard-yellow solid (0.197 g, 69%), m.p.: >250 ºC (decomp.) [49].

^{1}H NMR (400 MHz, DMSO-d_6) δ 8.49 (s, 2H), 8.47 (s, 2H), 7.88 (t, *J* = 8.0 Hz, 2H), 6.94 (d, *J* = 8.0 Hz, 2H), 6.64 (d, *J* = 8.0 Hz, 2H), 5.25 (s, 2H); ^{13}C NMR (101 MHz, DMSO-d_6) δ 164.0 (2C), 148.5, 134.2 (2C), 131.4, 130.7 (2C), 129.2 (2C), 127.4, 127.2 (2C), 123.8, 122.7 (2C), 113.7 (2C); IR (cm^{-1}) 3417 (NH_2), 3350 (NH_2), 3237 (Ar-H), 1652 (C=O), 779 (Ar-H); LCMS (ESI$^+$) m/z: 289 $[M+H]^+$ (100%).

*5-(1,3-Dioxo-1*H*-benzo[*de*]isoquinolin-2(3*H*)-yl)isophthalic acid (**24**)*

A solution of 1,8-naphthalic anhydride (1.0 mmol, 198 mg) was combined with 5-aminoisophthalic acid (1.0 mmol, 181 mg) and triethylamine (10 drops) in ethanol (15 mL) and was heated to reflux, with magnetic stirring, for 24 h. The mixture was filtered hot *in vacuo*. The resultant off-white solid was taken up in methanol (30 mL) and heated to boiling (100 °C) for 30 min. The mixture was filtered hot *in vacuo*, washed with cold ethanol (10 mL) and cold diethyl ether (2 x 10 mL), and dried *in vacuo* to afford the desired compound as an off-white solid (0.217 g, 60%), m.p.: >360 °C.

^{1}H NMR (400 MHz, DMSO-d_6) δ 13.41 (bs, 2H), 8.56 – 8.51 (m, 5H), 8.24 (s, 2H), 7.92 (t, *J* = 7.7 Hz, 2H); ^{13}C NMR (101 MHz, DMSO-d_6) δ 166.1 (2C), 163.6 (2C), 136.9, 134.50 (2C), 134.45 (2C), 132.2 (2C), 131.5, 130.7 (2C), 129.7, 128.0, 127.2 (2C), 122.7 (2C); IR (cm^{-1}) 3100-2500 (O-H), 1695 (C=O), 1668 (C=O), 772 (Ar-H); LCMS (ESI$^-$) m/z: 360 $[M-H]^-$ (100%); HRMS (ESI$^-$) m/z calculated for $C_{20}H_{10}NO_6$ $(M-H)^-$ 360.0514; found: 360.0503.

*5-(1,3-dioxo-1*H*-benzo[*de*]isoquinolin-2(3*H*)-yl)isophthalic acid, triethylammonium salt (**25**)*

1,8-naphthalic anhydride (1.0 mmol, 198 mg) was combined with 2-aminoterephthalic acid (1.0 mmol, 0.181 g) and triethylamine (10 drops) in 15 mL ethanol in a 10-20 mL microwave vial. A stirrer bar was added, the vial capped and the reaction mixture irradiated at 120 °C for 75 min. The reaction was cooled to 0 °C and a pale brown solid was isolated via vacuum filtration, washed with cold ethanol (3 mL) and cold diethyl ether (3 mL), and dried *in vacuo* to afford the desired compound as an eggshell-coloured solid (0.164 g, 35%), m.p. 215 °C (decomp.).

^{1}H NMR (400 MHz, DMSO) δ 8.55 – 8.47 (m, 4H), 8.03 (dd, *J* = 26.5, 8.1 Hz, 2H), 7.94 – 7.86 (m, 3H), 2.73 (q, *J* = 7.1 Hz, 6H), 0.94 (t, *J* = 7.2 Hz, 9H); ^{13}C NMR (101 MHz, DMSO-d_6) δ 167.1, 166.6, 163.8 (2C), 135.6, 135.4, 134.3 (2C), 132.5, 131.5, 131.2, 131.0, 130.5 (2C), 128.8, 128.0, 127.6, 127.2 (2C), 122.8, 44.9 (3C), 8.7 (3C); IR (cm^{-1}) 3000-2500 (O-H), 1709 (C=O), 1666 (C=O), 765 (Ar-H); LCMS (ESI$^-$) m/z: 360 $[M-H]^-$ (100%); HRMS (ESI$^-$) m/z calculated for $C_{20}H_{10}NO_6$ $(M-H)^-$ 360.0514; found: 360.0509.

*2-(2-Aminobenzyl)-1*H*-benzo[*de*]isoquinoline-1,3(2*H*)-dione (**26**)*

A solution of 1,8-naphthalic anhydride (1.0 mmol, 198 mg) was combined with 2-aminobenzylamine (3.0 mmol, 366 mg) and triethylamine (10 drops) in ethanol (15 mL) was heated to reflux, with magnetic stirring, for 44 h. After cooling to room temperature, the mixture was filtered *in vacuo*, and the pale brown solid was washed with cold ethanol (10 mL) and cold diethyl ether (2 x 10 mL), and dried *in vacuo* to afford the desired compound as a bright yellow solid (0.250 g, 80%), m.p.: 232-233 °C [27].

^{1}H NMR (400 MHz, $CDCl_3$) δ 8.59 (d, *J* = 7.4 Hz, 2H), 8.17 (d, *J* = 8.2 Hz, 2H), 7.73 (t, *J* = 7.8 Hz, 2H), 7.65 (d, *J* = 7.4 Hz, 1H), 7.07 (t, *J* = 7.2 Hz, 1H), 6.71 (t, *J* = 7.4 Hz, 1H), 6.65 (d, *J* = 7.9 Hz, 1H), 5.32 (s, 2H), 4.69 (s, 2H); ^{13}C NMR (101 MHz, $CDCl_3$) δ 165.1 (2C), 146.3, 134.3 (2C), 133.3, 131.7 (2C), 131.6, 129.3, 128.2, 127.1 (2C), 122.7 (2C), 121.3, 118.2, 116.3, 40.4; IR (cm^{-1}) 3413 (NH_2), 3344 (NH_2), 1692 (C=O); LRMS (ESI$^+$) *m/z* 303 $[M+H]^+$ (100%).

*2-(3-Aminobenzyl)-1*H*-benzo[*de*]isoquinoline-1,3(2*H*)-dione (**27**)*

A solution of 1,8-naphthalic anhydride (1.0 mmol, 198 mg) was combined with 3-aminobenzylamine (3.0 mmol, 366 mg) and triethylamine (10 drops) in ethanol (15 mL) was heated to reflux, with magnetic stirring, for 44 h. After cooling to room temperature, the mixture was filtered *in vacuo*, and the pale brown solid was washed with cold ethanol (10 mL) and cold diethyl ether (2 x 10 mL), and dried *in vacuo* to afford the desired compound as a pale tan solid (0.238 g, 79%), m.p.: 201-203 °C.

^{1}H NMR (400 MHz, $CDCl_3$) δ 8.59 (d, *J* = 7.8 Hz, 2H, H), 8.18 (d, *J* = 7.8 Hz, 2H), 7.73 (t, *J* = 7.8 Hz, 2H), 7.09 (t, *J* = 7.4 Hz, 1H), 6.95 (d, *J* = 7.4 Hz, 1H), 6.87 (s, 1H), 6.56 (d, *J* = 7.4 Hz, 1H), 5.30 (s, 2H), 3.62 (s, 2H); ^{13}C NMR (101 MHz, $CDCl_3$) δ 164.4 (2C), 146.6, 138.6, 134.1 (2C), 131.7, 131.5 (2C), 129.5, 128.3, 127.1 (2C), 122.8 (2C), 119.4, 115.6, 114.4, 43.6; IR (cm^{-1}) 3431 (NH_2), 3353 (NH_2), 1650 (C=O); LRMS (ESI$^+$) m/z: 303 $(M+H)^+$ (100%); HRMS (ESI$^+$) m/z calculated for $C_{19}H_{15}N_2O_2$ $(M+H)^+$ 303.1128; found: 303.1129.

*2-(4-Aminobenzyl)-1*H*-benzo[*de*]isoquinoline-1,3(2*H*)-dione (**28**)*

A solution of 1,8-naphthalic anhydride (1.0 mmol, 198 mg) was combined with 4-aminobenzylamine (3.0 mmol, 366 mg) and triethylamine (10 drops) in ethanol (15 mL) was heated to reflux, with magnetic stirring, for 20 h. After cooling to room temperature, the mixture was filtered *in vacuo*, and the pale brown solid was washed with cold ethanol (10 mL) and cold diethyl ether (2 x 10 mL), and dried *in vacuo* to afford the desired compound as a yellow solid (0.359 g, 95%), m.p.: > 250 °C (decomp.).

^{1}H NMR (400 MHz, DMSO-d_6) δ 8.49 (dd, *J* = 1.5, 7.2 Hz, 2H), 8.43 (dd, *J* = 1.5, 8.4 Hz, 2H), 7.85 (dd, *J* = 7.2, 8.4 Hz, 2H), 7.08 (d, *J* = 8.4 Hz, 2H), 6.46 (d, *J* = 8.4 Hz, 2H), 5.06 (s, 2H), 4.96 (bs, NH_2); ^{13}C NMR (101 MHz, DMSO-d_6) δ 163.5 (2C), 148.0, 134.5 (2C), 131.4, 131.0 (2C), 129.4 (2C), 127.4 (3C), 124.6, 122.1 (2C), 113.8 (2C), 42.7; IR (cm^{-1}) 3467 (NH_2), 3380 (NH_2), 1684 (C=O); LRMS (ESI$^+$) m/z: 303 $(M+H)^+$ (100%); HRMS (ESI$^+$) m/z calculated for $C_{19}H_{15}N_2O_2$ $(M+H)^+$ 303.1128; found: 303.1125.

*2-(2-Hydroxyethyl)-1*H*-benzo[*de*]isoquinoline-1,3(2*H*)-dione (**29**)*

1,8-naphthalic anhydride (1.0 mmol, 198 mg) was combined with ethanolamine (1.1 mmol, 0.084 mL) in 15 mL ethanol in a 10-20 mL microwave vial. A stirrer bar was added, the vial capped and the reaction mixture irradiated at 120 °C for 20 min. The reaction was cooled to 0 °C and a crystalline tan solid was isolated via vacuum filtration, washed with cold ethanol (3 mL) and cold diethyl ether (3 mL), and dried *in vacuo* to afford the desired compound as a tan crystalline solid (0.207 g, 86%), m.p.: 174-175 °C [27].

^{1}H NMR (400 MHz, DMSO-d_6) δ 3.61 (m, 2H), 4.14 (t, *J* = 6.6 Hz, 2H), 4.81 (t, *J* = 6.0 Hz, OH), 7.85 (dd, *J* = 7.5, 8.1 Hz, 2H), 8.44 (dd, *J* = 0.9, 8.1 Hz, H_2), 8.47 (dd, *J* = 0.9, 7.5 Hz, 2H); ^{13}C NMR (101 MHz, DMSO-d_6) δ 163.5 (2C), 134.2 (2C), 131.3, 130.6 (2C), 127.4, 127.2 (2C), 122.2 (2C), 57.8, 41.8; IR (cm^{-1}) 3300 (O-H), 2952 (C-H), 2861 (C-H), 1645 (C=O), 783 (Ar-H); LRMS (ESI$^+$) *m/z*: 242 $(M+H)^+$ (100%).

*2-(3-Hydroxypropyl)-1*H*-benzo[*de*]isoquinoline-1,3(2*H*)-dione (**30**)*

1,8-naphthalic anhydride (1.0 mmol, 198 mg) was combined with 3-amino-1-propanol (1.1 mmol, 0.084 mL) in 15 mL ethanol. The reaction was heated to 100 °C (reflux) for 18 hours. The reaction was cooled to room temperature and a pale brown solid was isolated via vacuum filtration, washed with cold ethanol (3 mL) and cold diethyl

ether (3mL) and dried *in vacuo* to afford the desired product as an off-white crystalline solid (0.209 g, 82%), m.p.: 121-123 °C.

^{1}H NMR (400 MHz, DMSO-d_6) δ 8.49 (d, *J* = 7.6 Hz, 2H), 8.45 (d, *J* = 7.6 Hz, 2H), 7.86 (t, *J* = 7.6 Hz, 2H), 4.49 (t, *J* = 5.2 Hz, 1H), 4.11 (t, *J* = 7.2 Hz, 2H), 3.50 (dd, *J* = 11.7, 6.2 Hz, 2H), 1.80 (q, *J* = 6.4 Hz, 2H); ^{13}C NMR (101 MHz, DMSO-d_6) δ 163.4 (2C), 134.3 (2C), 131.3, 130.7 (2C), 127.4, 127.2 (2C), 122.1 (2C), 59.0, 37.6, 31.0; IR (cm^{-1}) 3300 (O-H), 2952 (C-H), 2861 (C-H), 1645 (C=O), 783 (Ar-H); LRMS (ESI$^+$) *m/z*: 256 (M+H)$^-$ (100%); HRMS (ESI$^+$) m/z calculated for $C_{15}H_{14}NO_3$ (M+H)$^+$ 256.0968; found: compound did not ionise.

*2-(o-Tolyl)-1*H*-benzo[*de*]isoquinoline-1,3(2*H*)-dione (**31**)*

A solution of 1,8 naphthalic anhydride (**14**) (0.35 mmol, 0.070 g), *o*-toluidine (1.20 mmol, 0.128 g) and triethylamine (10 drops) in absolute ethanol (10 mL) was heated at reflux for 23 h, with magnetic stirring. The reaction was cooled to 0 ºC, and a brown solid was isolated by vacuum filtration, washed with cold ethanol (2 × 10 mL) and cold diethyl ether (2 × 5 mL) and dried *in vacuo* to afford the desired compound as a tan crystalline solid (0.034 g, 20%), m.p.: 217 ºC.

^{1}H NMR (400 MHz, DMSO-d_6) δ 8.55 (d, *J* = 2.4 Hz, 2H), 8.53 (d, *J* = 1.4 Hz, 2H), 7.93 (t, *J* = 8.0 Hz, 2H), 7.42 – 7.33 (m, 4H), 2.07 (s, 3H); ^{13}C NMR (101 MHz, DMSO-d_6) δ 163.3 (2C), 135.7 (2C), 135.2, 134.6 (2C), 131.5, 131.0 (2C), 130.4, 129.2, 128.5, 128.0, 127.3 (2C), 126.7, 122.3, 17.1; IR (cm^{-1}) 1656 (C=O), 1374 (C-H$_3$), 773 (Ar-H); LCMS (ESI$^+$) m/z: 288 [M+H]$^+$ (100%); HRMS (ESI$^+$) m/z calculated for $C_{19}H_{14}NO_2$ (M+H)$^+$ 288.1019; found: compound did not ionise.

*2-(Pyridin-2-yl)-1*H*-benzo[*de*]isoquinoline-1,3(2*H*)-dione (**32**)*

A solution of 1,8-naphthalic anhydride (**14**) (0.48 mmol, 0.097 g) and 2-aminopyridine (1.03 mmol, 0.097 g) in ethanol (7 mL) was heated to reflux, with magnetic stirring, for 36 h. The ensuing mixture was chilled; the resulting precipitate was subsequently collected *in vacuo*, washed with cold ethanol (10 mL) and cold diethyl ether (10 mL). The solid was then recrystallised from ethanol to afford the desired compound as a tan crystalline solid (0.030 g, 23%), m.p.: >250 ºC (decomp.).

^{1}H NMR (400 MHz, DMSO-d_6) δ 8.66 (dd, *J* = 5.2, 1.5 Hz, 1H), 8.54 (t, *J* = 8.3 Hz, 4H), 8.05 (td, *J* = 7.7, 1.9 Hz, 1H), 7.95 – 7.91 (m, 2H), 7.61 (dt, J = 7.9, 0.9 Hz, 1H), 7.55 (ddd, *J* = 7.5, 4.9, 1.1 Hz, 1H) ^{13}C NMR (101 MHz, DMSO-d_6) δ 163.5 (2C), 149.6 (2C), 149.4 (2C), 138.7, 134.8 (2C), 131.5, 130.8, 127.9, 127.3 (2C), 124.4, 124.2, 122.2; IR (cm^{-1}) 3072 (Ar-H), 1658 (C=O), 771 (Ar-H); LCMS (ESI$^+$) m/z: 275 [M+H]$^+$ (100%); HRMS (ESI$^+$) m/z calculated for $C_{17}H_{11}N_2O_2$ (M+H)$^+$ 275.0815; found: 275.0818.

*2-(2-Aminophenyl)isoquinoline-1,3(2*H*,4*H*)-dione (**33**)*

A solution of homophthalic anhydride (**7**) (1.17 mmol, 0.190 g) and *o*-phenylenediamine (2.60 mmol, 0.282 g) in absolute ethanol (15 mL) was heated to reflux, with magnetic stirring, for 18 h. Then, the ensuing mixture was cooled to room temperature. The precipitate was then collected by filtration *in vacuo*, washed with cold ethanol (2 × 10 mL) and cold diethyl ether (2 × 5 mL), and dried *in vacuo* to afford the desired compound as a white solid (0.127 g, 43%), m.p.: >250 ºC (decomp.).

^{1}H NMR (400 MHz, DMSO-d_6) δ 7.89 (d, *J* = 7.7 Hz, 1H), 7.51 (t, *J* = 7.5 Hz, 1H), 7.44 (dd, *J* = 6.0, 3.2 Hz, 2H), 7.38 (t, *J* = 7.1 Hz, 1H), 7.32 (d, *J* = 7.6 Hz, 1H), 7.10 (dd, *J* = 6.0, 3.2 Hz, 2H), 4.57 (s, 2H) (NH_2 not observed); ^{13}C NMR (101 MHz, DMSO-d_6) δ 168.4, 153.8, 138.7, 138.1 (2C), 131.8, 131.4, 130.7, 130.4, 126.8, 121.1 (2C), 114.5 (2C), 33.3; IR (cm^{-1}) 3059 (NH_2), 2914 (NH_2), 1635 (C=O), 783 (Ar-H); LCMS (ESI$^+$) m/z 253 [M+H]$^+$ (100%); HRMS (ESI$^+$) m/z calculated for $C_{15}H_{13}N_2O_2$ (M+H)$^+$ 253.0972; found: 253.0975.

*2-(1*H*-Benzo[*de*]isoquinolin-2(3*H*)-yl)aniline (**36**)*

To naphthalimide **22** (0.31 mmol, 0.091 g) was added sodium borohydride (1.6 mmol, 0.063 g), followed by THF (7 mL). To this solution was then added, dropwise, a solution of freshly sublimated iodine (1.04 mmol, 0.132 g) in tetrahydrofuran (7 mL), at room temperature, stirred magnetically. The mixture was then heated to 60 ºC for 18 h, at which point it was cooled to room temperature, then, treated with cold water (20 mL). The resultant solution was chilled to 0 ºC; the precipitate collected *in vacuo*, washed with water (10 mL), and dried *in vacuo* to afford the desired compound as an off-white solid (0.025 g, 31%), m.p.: >178 ºC (decomp.).

^{1}H NMR (400 MHz, DMSO-d_6) δ 7.79 (d, *J* = 8.1 Hz, 2H), 7.49 – 7.43 (m, 2H), 7.32 (d, *J* = 6.9 Hz, 2H), 7.02 (d, *J* = 7.8 Hz, 1H), 6.88 – 6.82 (m, 1H), 6.73 (dd, *J* = 7.9, 1.4 Hz, 1H), 6.56 (td, *J* = 7.6, 1.5 Hz, 1H), 4.73 (s, 2H), 4.37 (s, 4H); ^{13}C NMR (101 MHz, DMSO-d_6) δ 142.6, 137.4, 134.1 (2C), 132.7, 127.6, 125.8 (2C), 125.7 (2C), 124.3, 121.7 (2C), 119.7, 116.6, 114.5, 53.9 (2C); IR (cm^{-1}) 3443 (N-H$_2$), 3345 (N-H$_2$), 1606 (N-H$_2$), 765 (Ar-H); LCMS (ESI$^+$) m/z: 261 [M+H]$^+$ (100%); HRMS (ESI$^+$) m/z calculated for $C_{18}H_{17}N_2$ (M+H)$^+$ 261.1386; found: 261.1388.

Acknowledgements

JRB is the recipient of an Australia government HDR scholarship. Funding from the Australian Cancer Research Foundation and the Ramaciotti Foundation is gratefully acknowledged. SP is the recipient of a Fulbright Senior Scholar Fellowship.

Keywords: naphthalimides • aryl hydrocarbon receptor • breast cancer • homology modelling • molecular dynamics

References:

[1] C. X. Ma, T. Reinert, I. Chmielewska, M. J. Ellis, Nat. Rev. Cancer 2015, 15, 261–275.
[2] J. S. Park, J.-C. Youn, C. Y. Shim, G.-R. Hong, C.-K. Lee, J. H. Kim, H. S. Park, S. J. Heo, S. H. Beom, H. S. Kim, et al., Oncotarget 2017, 8, 61837–61845.
[3] F. Schettini, G. Buono, C. Cardaseli, I. Desideri, S. De Placido, L. Del Mastro, Can. Treat. Rev. 2016, 46, 20-26.
[4] P. Sharma, The Oncologist 2016, 21, 1050–1062.
[5] P. S. Steeg, Nat. Rev. Cancer 2016, 16, 201–218.
[6] A. B. Okey, Toxicological Sciences 2007, 98, 5–38.
[7] V. P. Androutsopoulos, A. M. Tsatsakis, D. A. Spandidos, BMC Cancer 2009, 9, 187.
[8] A. A. Walsh, G. D. Szklarz, E. E. Scott, J Biol Chem 2013, 288, 12932–12943.
[9] S. K. Kolluri, U.-H. Jin, S. Safe, Arch. Toxicol. 2017, 91, 2497–2513.
[10] M. S. Denison, S. R. Nagy, Annu. Rev. Pharmacol. Toxicol. 2003, 43, 309–334.
[11] I. A. Murray, A. D. Patterson, G. H. Perdew, Nat. Rev. Cancer 2014, 14, 801–814.
[12] J. Tian, Y. Feng, H. Fu, H. Q. Xie, J. X. Jiang, B. Zhao, Environ. Sci. Technol. 2015, 49, 9518–9531.
[13] D. Dolciami, M. Ballarotto, M. Gargaro, L. C. López-Cara, F. Fallarino, A. Macchiarulo, Eur. J. Med. Chem. 2020, 185, 111842.
[14] M. Tarleton, J. Gilbert, M. J. Robertson, A. McCluskey, J. A. Sakoff, Med. Chem. Commun. 2011, 2, 31.
[15] J. Gilbert, G. N. De Iuliis, M. Tarleton, A. McCluskey, J. A. Sakoff, Mol. Pharmacol. 2018, 93, 168–177.
[16] A. Al Otaibi, C. P. Gordon, J. Gilbert, J. A. Sakoff, A. McCluskey, RSC Adv. 2014, 4, 19806–19813.

[17] M. Tarleton, J. Gilbert, J. A. Sakoff, A. McCluskey, Eur. J. Med. Chem. 2012, 57, 65–73.
[18] M. Tarleton, L. Dyson, J. Gilbert, J. A. Sakoff, A. McCluskey, Bioorg. Med. Chem. 2013, 21, 333–347.
[19] M. Tarleton, J. Gilbert, J. A. Sakoff, A. McCluskey, 2012, 57, 65–73.
[20] J. R. Baker, J. Gilbert, S. Paula, X. Zhu, J. A. Sakoff, A. McCluskey, ChemMedChem. 2018, 14, 1447-1458.
[21] J. Gilbert, G. N de Iuliis, A. McCluskey, J. A. Sakoff, Sci. Rep. 2020, 10, 13978. Doi.org/10.1038/s41598-020-70597-8
[22] E. Brantley, M. A. Callero, D. E. Berardi, P. Campbell, L. Rowland, D. Zylstra, L. Amis, M. Yee, M. Simian, L. Todaro, A. I. Loaiza-Perez, U. Soto, Cancer Lett. 2016, 376, 53-61.
[23] A. K. Ehrlich, J. M. Pennington, X. Wang, D. Rohlman, S. Punj, C. V. Löhr, M. T. Newman, S. K. Kolluri, N. I. Kerkvliet, Jour. Immun. 2016, 196, 264-273.
[24] M. A. Callero, A. I. L. Perez, Int. J. Breast Cancer. 2011, 2011, 923250.
[25] S. Punj, P. Kopparapu, H. S. Jang, J. L. Phillips, J. Pennington, Diana Rohlman, E. O'Donnell, P. L. Iversen, S. K. Kolluri, N. I. Kerkvliet, PLoS ONE 2014, 9, e88726
[26] K. A. MacGregor, M. J. Robertson, K. A. Young, L. von Kleist, W. Stahlschmidt, A. Whiting, N. Chau, P. J. Robinson, V. Haucke, A. McCluskey, J. Med Chem. 2014, 57, 131-143.
[27] K. A. MacGregor, A. McCluskey, Tet. Lett. 2011, 52, 767-769.
[28] M. K. Abdel-Hamid, K. A. MacGregor, L. R. Odell, N. Chau, A. Mariana, A. Whiting, P. J. Robinson, A. McCluskey, Org. Biomol. Chem. 2015, 13, 8016-8028.
[29] T. A. Hill, S. G. Stewart, S. P. Ackland, J. Gilbert, B. Sauer, J. A. Sakoff, A. McCluskey, Bioorg. Med. Chem. 2007, 15, 6126-6134.
[30] S. Paula, J. R. Baker, X. Zhu, A. McCluskey, in *Computational Docking and Molecular Dynamics Simulations, Molecular Docking and Molecular Dynamics*, Amalia Stefaniu, IntechOpen, DOI: 10.5772/intechopen.84818.
[31] A. M. Bergman, V. W. R. van Haperen, G. Veerman, C. M. Kuiper, G. J. Peters, Clin. Cancer Res. 1996, 2, 521–530.
[32] J. A. Sakoff, S. P. Ackland, Cancer Chemother. Pharmacol. 2000, 46, 477–487.
[33] N. Huang, Y. Chelliah, Y. Shan, C. A. Taylor, S.-H. Yoo, C. Partch, C. B. Green, H. Zhang, J. S. Takahashi, Science 2012, 337, 189–194.
[34] H. A. King, A. Hoelz, B. R. Crane, M. W. Young, J. Mol. Biol. 2011, 413, 561–572.
[35] T. H. Scheuermann, D. R. Tomchick, M. Machius, Y. Guo, R. K. Bruick, K. H. Gardner, Proc. Natl. Acad. Sci. U.S.A. 2009, 106, 450–455.
[36] J. Key, T. H. Scheuermann, P. C. Anderson, V. Daggett, K. H. Gardner, J. Am. Chem. Soc. 2009, 131, 17647–17654.
[37] J. C. Phillips, R. Braun, W. Wang, J. Gumbart, E. Tajkhorshid, E. Villa, C. Chipot, R. D. Skeel, L. Kalé, K. Schulten, J. Comput. Chem. 2005, 26, 1781–1802.
[38] T. Darden, D. York, L. Pedersen, J. Chem. Phys. n.d., 98, 10089–10092.
[39] G. J. Martyna, D. J. Tobias, M. L. Klein, J. Chem. Phys. 1994, 101, 4177–4189.
[40] H. C. Anderson, Jour. Comp. Phys. 1983, 52, 24–34.
[41] W. Humphrey, A. Dalke, K. Schulten, J Mol Graph 1996, 14, 33–38.
[42] J. Huang, S. Rauscher, G. Nawrocki, T. Ran, M. Feig, B. L. de Groot, H. Grubmüller, A. D. MacKerell, Nat. Methods. 2017, 14, 71–73.
[43] S. R. Durell, B. R. Brooks, A. Ben-Naim, 1994, J. Phys. Chem. n.d., 98, 2198–2202.
[44] W. L. Jorgensen, J. Chandrasekhar, J. D. Madura, R. W. Impey, M. L. Klein, J. Chem. Phys. 1998, 79, 926–935.
[45] E. Neria, S. Fischer, M. Karplus, J. Chem. Phys. 1998, 105, 1902–1921.
[46] K. Vanommeslaeghe, E. Hatcher, C. Acharya, S. Kundu, S. Zhong, J. Shim, E. Darian, O. Guvench, P. Lopes, I. Vorobyov, A. D. Mackerel, J. Comput. Chem. 2010, 31, 671–690.
[47] C. S. Keenan, S. S. Murphree, Synth. Commun. 2017, 47, 1085–1089.
[48] A. R. K. Murphy, J. M. Chapman, S. D. Wyrick, I. H. Hall, Pharm. Res. 1986, 3, 286-289.
[49] C. S. Choi, K. S. Jeon, W. C. Jeong, K. H. Lee, Bull. Korean. Chem. Soc. 2010, 31, 1375-1376.
[50] A. Takács, P. Ács, L. Kollár, Tetrahedron. 2008, 64, 983-987.
[51] I. I. Ponomarev, M. U. Zharinova, Z. S. Klemenkova, P. V. Petrovskii, Z. A. Starikova, Russ. Chem. Bull., Int. Ed. 2011, 60, 512-520.
[52] Q. Song, A. Bamesberger, L. Yang, H. Houtwed, H. Cao, Analyst. 2014, 139, 3588-3592.

Entry for the Table of Contents

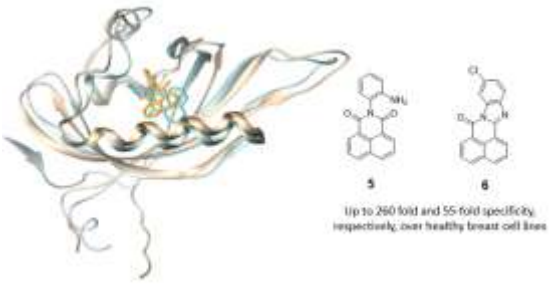

Targeting the aryl hydrocarbon receptor reveals novel breast cancer cytotoxic specific small molecules.